Proceedings of the 23rd International Conference on Automation & Computing, University of Huddersfield, Huddersfield, UK, 7-8 September 2017

Planetary Gearbox Fault Diagnosis Using an On-Rotor MEMS Accelerometer

Mones Z. [a], Zeng Q. [a,b], Hu L. [a], Tang X. [a], , Gu F. [a] and Ball A. D. [a]

[a] University of Huddersfield
Huddersfield, UK
[b] State Key Laboratory of Mechanical Transmission
Chongqing University
Chongqing, People's Republic of China
Zainab.Mones@hud.ac.uk

Abstract—**Conventional accelerometers installed on housing often give out less accurate diagnostic results for planetary gearbox because the mesh excitation of planet gears change with carrier movement. Recent significant advancements in low-power and low-cost Micro-Electro-Mechanical Systems (MEMS) technologies make it possible and easier to mount MEMS accelerometers directly on the rotating shaft, enabling more accurate dynamic characteristics of the rotating machine to be acquired and used for condition monitoring. In this paper, two tiny MEMS accelerometers are installed diametrically opposite each other on the low-speed input shaft of a planetary gearbox to measure the acceleration signals. The acceleration signals sensed by each MEMS will contain both the tangential acceleration and gravitational acceleration, but the latter can be removed by summing the acceleration signals from both sensors in order to characterise the rotor dynamics precisely. The experimental results show that the tangential acceleration measured on the low-speed input shaft of a planetary gearbox can clearly indicate faults, thus providing a reliable and low-cost method for planetary gearbox condition monitoring.**

Keywords—MEMS accelerometer; on-rotor measurement; planetary gearbox; condition monitoring

I. INTRODUCTION

Planetary gearboxes are widely used in drivetrains of helicopters, wind turbines and automotive and heavy industry applications due to their large transmission ratio, strong load-bearing capacity and high transmission efficiency [1, 2]. Since the applications of planetary gearboxes are quite critical and their failure may cause shutdown of the entire train resulting in major economic losses, condition monitoring of planetary gearboxes has received significant attention from many researchers. To avoid any unexpected interruptions and accidents that might be caused by planetary gearbox failure [3, 4]. , many studies have recently been carried out into the development of planetary gearbox condition monitoring and fault diagnosis. A review study on the methodologies of planetary gearbox condition monitoring and fault diagnosis is presented in [4] and, according to this study, most planetary gearbox diagnostic systems have used the vibration signal measured by an accelerometer mounted on the housing of the planetary gearbox. Generally, this vibration signal, $z(t)$, contains valuable diagnostic information regarding the planetary gear-set, and can be considered as the superposition of vibrations from planets meshing with the annulus and sun gear [5].

$$z(t) = \sum_{i=1}^{p} \omega_i(t)\left[x_i(t)+y_i(t)\right] \quad (1)$$

The signal $x_i(t)$, in Equation (1), denotes the vibration resulting from the gear and i^{th} planet mesh, which is periodic at the fundamental gear mesh frequency f_m, whilst the $y_i(t)$ indicates the vibration resulting from the sun gear and i^{th} planet mesh, which is also periodic at the fundamental gear mesh frequency f_m. The window function $\omega_i(t)$ is used to describe the amplitude modulation phenomenon caused by the relative motion between the fixed accelerometer and the rotating planets within the carrier [5, 6]. This phenomenon can be explained as follows: as a planet rotates and becomes closer to the fixed accelerometer, its vibration dominates the sensory data and the level of its impact reaches a peak when the planet is almost under the accelerometer; thereafter, it decreases as the planet moves away from the accelerometer. As a result, the sidebands in the measured vibration signal sensed by a fixed accelerometer have a complex nature, which makes the application of conventional vibration-based diagnostic techniques to planetary gearboxes a challenge [5]. This issue can be solved by employing an accelerometer directly on the rotating shaft, providing a constant distance between the accelerometer and the rotating planets.

With rapid developments in Micro-Electro-Mechanical Systems (MEMS) technology, it has become feasible to install a low-cost MEMS accelerometer directly onto the rotating part to measure the on-rotor acceleration used for rotating machine condition monitoring and fault diagnosis [7]. Furthermore, as the MEMS accelerometer is directly attached to a rotor, it is able to accurately capture the dynamic characteristics of the rotating part [8, 9], which makes it a good alternative to an expensive conventional accelerometer. Many researchers have recently paid attention to this usage of an on-rotor MEMS accelerometer for rotating condition monitoring and fault diagnosis. For example, Arebi et al. studied and compared responses from data collected via an on-rotor MEMS accelerometer and a

shaft encoder under different degrees of shaft misalignment, and the findings showed that the MEMS accelerometer outperformed the shaft encoder in detecting small shaft misalignment [8]. Baghli et al. developed a new kind of instantaneous torque sensor based on a MEMS accelerometer. They installed two MEMS accelerometers on the coupling of a rotor shaft to acquire the instantaneous torque measurements used for induction motor condition monitoring, and the study proved the effectiveness and accuracy of using on-rotor MEMS accelerometers to measure instantaneous torque [10]. Jiménez et al. introduced a novel topology for enhanced vibration sensing, whereby a MEMS accelerometer was embedded within a hollow rotor allowing the rotational speed to be measured. The speed estimation algorithm presented in that study was tested on a rotor operating at a range of speeds between 200 RPM and 2000 RPM and, by comparing the results obtained using the MEMS accelerometer with the speed measured by the encoder, they confirmed that their method was robust and could be applied to rotors irrespective of the state of vibration and during both acceleration and deceleration [11]. As the authors of [7, 12] explain, one of the most critical issues in using on-rotor MEMS accelerometers is obtaining the pure tangential acceleration from accelerometer outputs which also contain gravitational acceleration, in order to characterise the rotor dynamics precisely and use them for condition monitoring. In [7], they mounted a three-axial MEMS data logger on the flywheel of a reciprocating compressor to record the on-rotor accelerations. By combining the acceleration from two axes, the gravitational acceleration was successfully eliminated and the accurate tangential acceleration signals were reconstructed and used for reciprocating compressor condition monitoring.

This paper uses MEMS accelerometers installed on a low-speed input shaft to measure the acceleration signals used for planetary gearbox condition monitoring and fault diagnosis.

II. GRAVITY CANCELLATION USING TWO MEMS ACCELEROMETERS

AX3 data logger used in this work is essentially constructed with a low cost and low power ADXL345 located at the heart of Ax3 and connected with a large block NAND flash memory chip. ADXL345 is small, three-axis accelerometer with high resolution (13-bit) with measurement range up to ±16g. It measures the dynamic acceleration resulting from motion as well as the static acceleration of gravity [12]. Therefore, the signals measured using on-rotor MEMS accelerometers contain the required rotor dynamic information as well as the gravitational accelerations, which have to be removed to obtain the rotor dynamics precisely. Fig. 1 shows the block diagram of ADXL345 MEMS accelerometer.

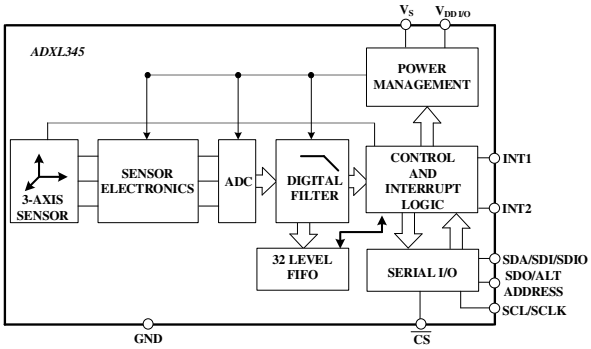

Figure 1. Accelerometer block diagram

As shown in Fig. 2, this paper has used two MEMS accelerometers mounted diametrically opposite each other, allowing the gravitational acceleration signal to be cancelled by summing the Y-axis signals from both MEMS sensors [13]. Based on Fig. 2, the Y output signals for both sensors *A* and *B* can be expressed as:

$$\begin{aligned} a_{Ax} &= -a_c + g_x = -a_c + g\sin\theta \\ a_{Ay} &= a_t + g_y = a_t + g\cos\theta \\ a_{Bx} &= a_c + g_x = a_c + g\sin\theta \\ a_{By} &= a_t - g_y = a_t - g\cos\theta \end{aligned} \tag{2}$$

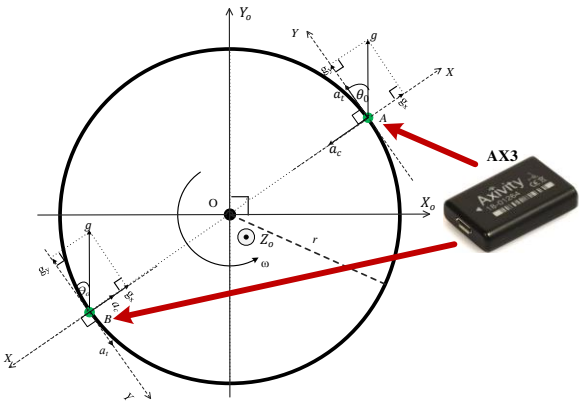

Figure 2. Acceleration analysis of two masses (A and B) rotating around point O

From Equation (2), it can be noticed that gravity appears in both the X-axis and Y-axis outputs, but by summing a_{Ay} and a_{By}, this undesirable signal can be eliminated and the tangential acceleration can be obtained as:

$$a_{Ay} + a_{By} = 2a_t \tag{3}$$

Then, the pure tangential acceleration that characterises the rotor dynamics can be expressed as:

$$a_t = \frac{a_{Ay} + a_{By}}{2} \tag{4}$$

According to Equation (4), this is an easy and direct way to eliminate the gravitational acceleration. However, there are some disadvantages of removing the undesirable signals using this method. Firstly, it is more expensive; secondly, it is difficult to install the MEMS accelerometers in the precise positions and finally, the sampling rates for the two MEMS accelerometers may be slightly different, which means that more post-processing is required. In this experimental work, both AX3 data logger sensors were configured to operate with a sampling rate of 1600 Hz. However, the actual sampling frequencies for these sensors were calculated and the findings were slightly different from the configured value. For the first AX3, the actual sampling frequency was 1590 Hz, while it was 1610 Hz for the other sensor. The sampling rate can be corrected by taking the following steps:

- Synchronise both sensors' data to the same time.
- Divide both sets of data into many frames.
- Resample the sensors' data based on the frames.

III. PLANETARY GEARBOX CHARACTERISTIC FREQUENCIES FOR FAULT DIAGNOSIS

Fig. 3 shows a typical configuration of the planetary gearbox employed in the present work. It includes three planet gears, a planet gear carrier connected with the input, a central sun gear assumed to be connected with the output shaft and lastly, a ring gear fixed within the gear housing.

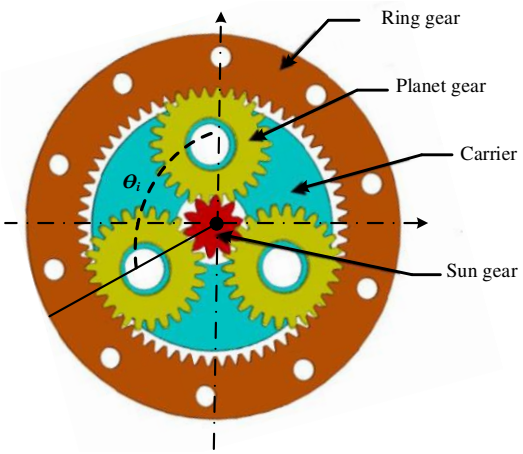

Figure 3. Planetary gearbox schematic

Many studies have shown that any type of fault in the planetary gearbox will lead to the development of mechanical vibrations, and by examining the changes in characteristic frequency spectrum around the mesh frequency and its harmonics, these faults can be detected and diagnosed [3]. Assuming that K is the number of planetary gears that are moving within the carrier, the characteristic vibration frequencies around the meshing frequency are unique for each type of planetary gearbox fault, as identified by [4].

A. *Characteristic Frequency of Sun Gear with Local Fault*

Assuming that there is a local fault on the sun gear and the system starts rotating, the vibration signal will have two different conditions. When the local fault overlaps with one of the planet gears, the vibration signal will be modulated by an impulse signal, and when the local fault leaves the meshing area, the vibration signal will return to its normal condition [14]. This modulating phenomenon happens K times in one revolution of the sun gear. In the ideal case of an error-free manufacture, the characteristic frequency of a sun gear with a local fault , f_{sf}, can be given as:

$$f_{sf} = \frac{f_m}{z_s} = K\left(f_{rs} - f_{rc}\right) \tag{5}$$

where K is the planet gear number.

B. *Characteristic Frequency of Planet Gear with Local Fault*

When a local fault occurs on both sides of the planet gear tooth, the vibration signal modulation happens twice during its one period revolution. Then, the characteristic frequency of the planet gear with local fault f_{pf} can be expressed as:

$$f_{pf} = 2\frac{f_m}{z_p} = 2\left(f_{rp} + f_{rc}\right) \tag{6}$$

C. *Characteristic Frequency of Ring Gear*

Similar to the result from the sun gear with local fault frequencies, the characteristic frequency of a ring gear with local fault f_{rf} can be calculated as:

$$f_{rf} = \frac{f_m}{z_r} = Kf_{rc} \tag{7}$$

For the planetary gearbox used in this work, Z_s is the number of sun gear teeth=10, Z_p is the number of the three planet gears' teeth=26 and Z_r is the number of ring gear teeth=62.

IV. EXPERIMENTAL VALIIDATION

A. *Test rig-setup*

Fig. 4 shows a schematic diagram of the planetary gearbox test rig used in this experimental study. It mainly consists of a three phase induction motor of 11 kW 1465rpm, a two-stage helical gearbox, a planetary gearbox manufactured by STM Power Transmission Ltd, two flexible tyre couplings and a DC generator for providing load to the gearbox. The running state of the planetary gearbox was monitored using on-rotor MEMS accelerometers. The input shaft of the planetary gearbox was driven by an induction motor, the speed of which was regulated by a speed controller with a maximum speed of up to 40% ≈ 584 rpm. This means the input speed to the planetary gearbox was reduced by the helical gearbox, with a ratio of 3.667 to 159 rpm, and thereafter the speed was increased to 1144 rpm by the planetary gearbox with a ratio of 7.2.

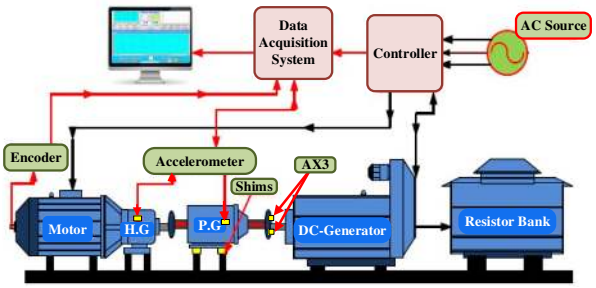

Figure 4. Schematic diagram of planetary gearbox test facility

Figure 5. Planetary gearbox test rig and

As shown in Fig. 5, two AX3 data logger sensors are mounted diametrically opposite each other on the low speed input shaft of a planetary gearbox and close to the centre to record the on-rotor acceleration signals. The holders for the MEMS sensors were designed using SolidWorks CAD software, which is one of the best methods for 3D modelling, and printed out using a 3D printer.

B. Faults simulation

In this study, two different areas of damage were simulated in both the sun and planet gears in order to simulate real faults in the mechanism during operation. Fig. 6 (a) shows the damage in the sun gear produced by removing around 60% of the tooth face on the gear in the width direction, whilst the damage created in the planet gear by also removing parts of the tooth is presented in Fig. 6 (b).

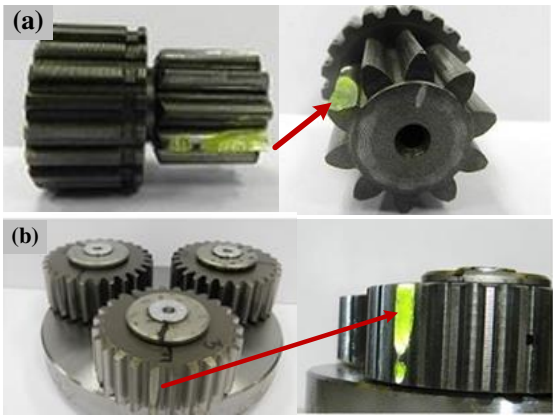

Figure 6. Fault simulated on (a) the sun gear and (b) planet gear.

C. Test Procedure

Before the test, both AX3 data logger sensors were configured to operate with a dynamic range of ±16g and a sampling rate of 1600 Hz to allow sufficient inspection of the rotor dynamic characteristics. The collected data were stored in memory during machine run-time, and then exported for post-processing after the machine was shut down. In this work, three different groups of data have been collected to evaluate the performance of the AX3 accelerometers. The first data are healthy (BL), having been acquired when the system was operating under normal conditions with no faults. Two more groups of data have been collected from the system with separate areas of damage created on the sun gear and planet gear teeth. For each condition, the test was carried out at speeds of 30% of the full speed of the AC motor (439.5 rpm) and under different loads, including zero load and 25%, 50%, 75% and 90% of the full load.

V. Results and Discussion

Fig. 7 shows typical sets of outputs on the X-axis for both AX3 sensors with their spectra at 30% speed and 90% load when the system was working under normal conditions. By summing these signals, the gravitational acceleration can be eliminated and the tangential acceleration is obtained and presented in Fig. 8.

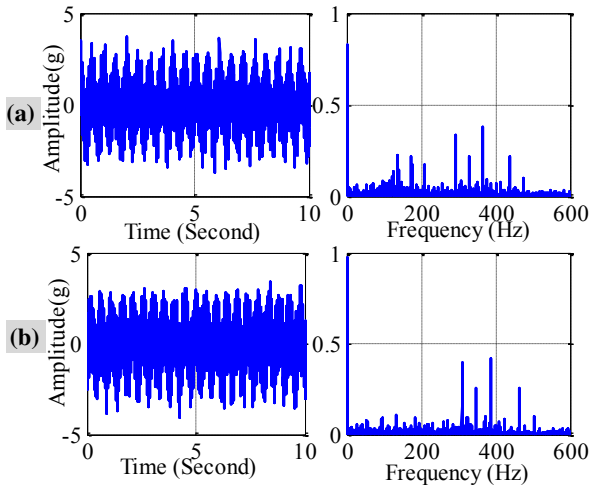

Figure 7. X-axis filtered acceleration signals and its spectra with 90% load and 30% speed for (a) Sensor 1 and (b) Sensor 2

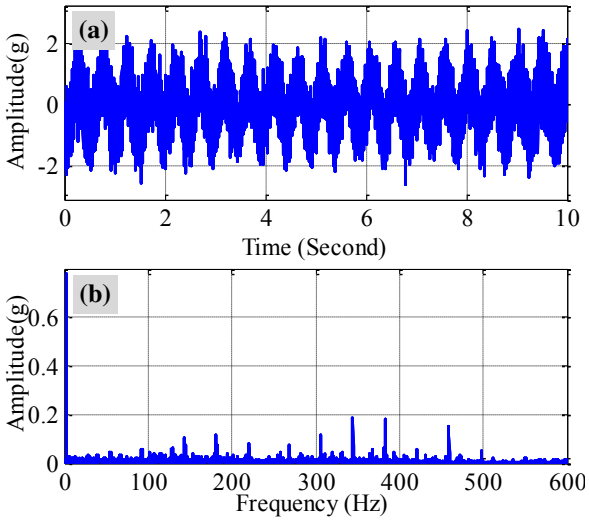

Figure 8. Tangential acceleration signal and spectra at 30% speed and90% load

After zooming in Fig. 8 (b) and a closer inspection we noticed that the largest frequency component for tangential

acceleration is situated at around 2.067 Hz, which represents the steady angular speed of the carrier, and this value is taken as the fundamental frequency of the low-speed input shaft.

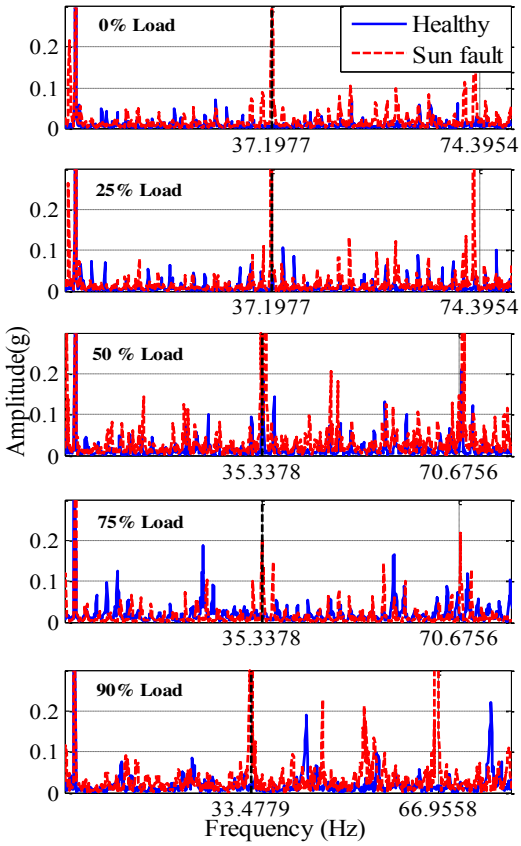

Figure 9. Spectrum in the low frequency range for the healthy and sun fault cases at 30% speed

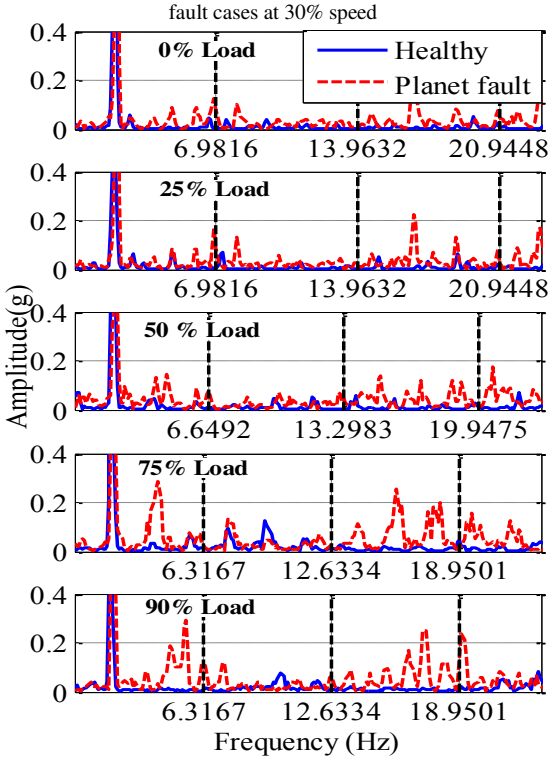

Figure 10. Spectrum in the low frequency range for the healthy and plant fault cases at 30% speed

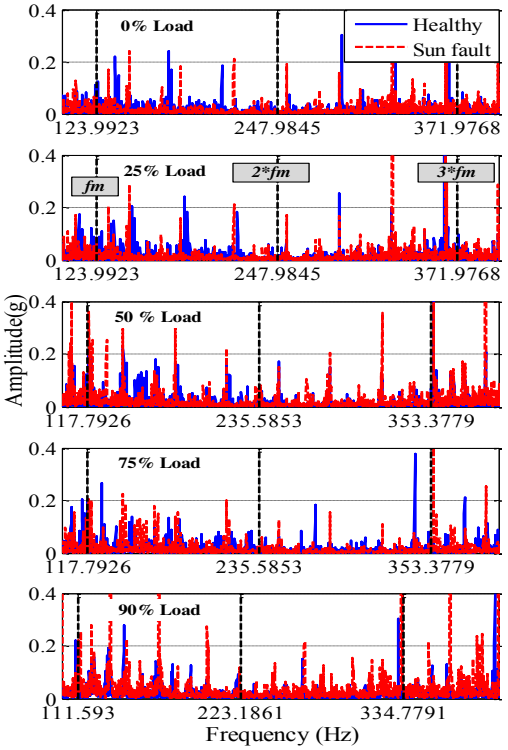

Figure 11. Spectrum in the high frequency range for the healthy and sun fault cases

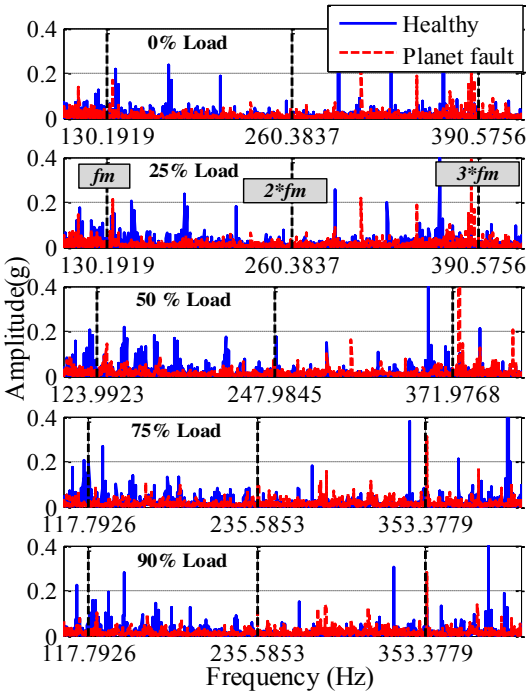

Figure 12. Spectrum in the high frequency range for the healthy and plant fault cases

Fig. 9 and Fig. 10 show the low frequency spectra of the tangential acceleration measured at 30% speed with different loads for the sun fault condition and planet fault case respectively. From these figures, it can be seen that the frequency spectrum amplitudes were impacted by the damage and many frequency components appeared such as f_{sf} and f_{pf} which means these frequencies can be used to indicate the sun gear fault and planet fault.

To investigate the impact of the sun and planet damage created in the planetary gearbox more closely, the high frequency spectra for the tangential acceleration sensed at 30% speed with different loads are presented in Fig. 11 and Fig. 12.

In both cases, the amplitude of frequencies around the mesh frequency harmonics (f_m) was generally higher than that of the low frequency range sections. Many previous researchers have studied the high frequency spectra of vibration signals sensed by a fixed accelerometer, and most of these studies have concluded that sideband signals around the 3rd harmonics of the mesh frequency can be effectively used to indicate different faults. From Fig. 11 and Fig. 12, it is clear that the sidebands around the 3rd mesh frequency harmonic is higher compared with the 1st and 2nd harmonics. The sidebands around the 3rd mesh frequency harmonic were examined and some distinctive peak components were found which could be used for fault diagnosis. For example, $3f_m+f_{rc}$, $3f_m+2f_{rc}$, $3f_m-f_{sf}$, $3f_m+f_{sr}$, $3f_m-f_{sf,}+f_{rc}$, and $3f_m+f_{sf,}+f_{rc}$ could be useful to indicate the sun fault, whilst, $3f_m-3f_{pf}$, $3f_m+10f_{pf}$, *and* $3f_m-6f_{pf}-f_{rc}$ can successfully indicate the planet fault.

VI. Conclusion

This paper has introduced a new method for planetary gearbox condition monitoring. It is based on MEMS accelerometers installed on the shaft to measure the on-rotor dynamics. Based on the results, which allows a good indication of both the sun gear fault and the planet gear fault, it can be concluded that this method can be used for low-cost condition monitoring and fault diagnosis.

In further study, the method presented in this paper will be devolved by improving on the data collection method using wireless transmission technique allowing accelerations data to be acquired and sent remotely to a host computer or to the cloud.

References

[1] Lei, Y., D. Han, J. Lin, and Z. He, Planetary gearbox fault diagnosis using an adaptive stochastic resonance method. Mechanical Systems and Signal Processing, 2013. 38(1): p. 113-124.

[2] Yoon, J., D. He, B. Van Hecke, T.J. Nostrand, J. Zhu, and E. Bechhoefer. Planetary Gearbox Fault Diagnosis Using a Single Piezoelectric Strain Sensor. in 2014 Annual Conference of the Prognostics and Health Management Society, PHM 2014. Prognostics and Health Management Society.

[3] Gu, F., G.M. Abdalla, R. Zhang, H. Xun, and A. Ball, A Novel Method for the Fault Diagnosis of a Planetary Gearbox based on Residual Sidebands from Modulation Signal Bispectrum Analysis. 2014.

[4] Lei, Y., J. Lin, M.J. Zuo, and Z. He, Condition monitoring and fault diagnosis of planetary gearboxes: A review. Measurement, 2014. 48: p. 292-305.

[5] Hong, L., Y. Qu, Y. Tan, M. Liu, and Z. Zhou, Vibration Based Diagnosis for Planetary Gearboxes Using an Analytical Model. Shock and Vibration, 2016.

[6] Inalpolat, M. and A. Kahraman, A dynamic model to predict modulation sidebands of a planetary gear set having manufacturing errors. Journal of Sound and Vibration, 2010. 329(4): p. 371-393.

[7] Feng, G., N. Hu, Z. Mones, F. Gu, and A. Ball, An investigation of the orthogonal outputs from an on-rotor MEMS accelerometer for reciprocating compressor condition monitoring. Mechanical Systems and Signal Processing, 2016. 76: p. 228-241.

[8] Arebi, L., F. Gu, N. Hu, and A. Ball, Misalignment detection using a wireless sensor mounted on a rotating shaft. 2011.

[9] Feng, G., N. Hu, Z. Mones, F. Gu, and A.D. Ball, An investigation of the orthogonal outputs from an on-rotor MEMS accelerometer for reciprocating compressor condition monitoring. Mechanical Systems and Signal Processing, 2016. 76–77: p. 228-241.

[10] Baghli, L., J.F. Pautex, and S. Mezani. Wireless instantaneous torque measurement, application to induction motors. in Electrical Machines (ICEM), 2010 XIX International Conference on. 2010. IEEE.

[11] Jiménez, S., M.O. Cole, and P.S. Keogh, Vibration sensing in smart machine rotors using internal MEMS accelerometers. Journal of Sound and Vibration, 2016. 377: p. 58-75.

[12] Mones, Z., G. Feng, U.E. Ogbulaor, T. Wang, F. Gu, and A.D. Ball, Performance evaluation of wireless MEMS accelerometer for reciprocating compressor condition monitoring, in Power Engineering. 2016, CRC Press. p. 893-900.

[13] Thompson, H. Wireless sensor research at the rolls-royce control and systems university technology centre. in Wireless Communication, Vehicular Technology, Information Theory and Aerospace & Electronic Systems Technology, 2009. Wireless VITAE 2009. 1st International Conference on. 2009. IEEE.

[14] Miao, Q. and Q. Zhou, Planetary gearbox vibration signal characteristics analysis and fault diagnosis. Shock and Vibration, 2015.